

# Effective Static Approximation: A Fast and Reliable Tool for Warm Dense Matter Theory

Tobias Dornheim,<sup>1,\*</sup> Attila Cangi,<sup>1</sup> Kushal Ramakrishna,<sup>2,3</sup>  
Maximilian Böhme,<sup>1,3</sup> Shigenori Tanaka,<sup>4</sup> and Jan Vorberger<sup>2</sup>

<sup>1</sup>*Center for Advanced Systems Understanding (CASUS), D-02826 Görlitz, Germany*

<sup>2</sup>*Helmholtz-Zentrum Dresden-Rossendorf (HZDR), D-01328 Dresden, Germany*

<sup>3</sup>*Technische Universität Dresden, D-01062 Dresden, Germany*

<sup>4</sup>*Graduate School of System Informatics, Kobe University, Kobe 657-8501, Japan*

We present an *Effective Static Approximation* (ESA) to the local field correction (LFC) of the electron gas that enables highly accurate calculations of electronic properties like the dynamic structure factor  $S(q, \omega)$ , the static structure factor  $S(q)$ , and the interaction energy  $v$ . The ESA combines the recent neural-net representation [*J. Chem. Phys.* **151**, 194104 (2019)] of the temperature dependent LFC in the exact static limit with a consistent large wave-number limit obtained from Quantum Monte-Carlo data of the on-top pair distribution function  $g(0)$ . It is suited for a straightforward integration into existing codes. We demonstrate the importance of the LFC for practical applications by re-evaluating the results of the recent X-ray Thomson scattering experiment on aluminum by Sperling *et al.* [*Phys. Rev. Lett.* **115**, 115001 (2015)]. We find that an accurate incorporation of electronic correlations in terms of the ESA leads to a different prediction of the inelastic scattering spectrum than obtained from state-of-the-art models like the Mermin approach or linear-response time-dependent density functional theory. Furthermore, the ESA scheme is particularly relevant for the development of advanced exchange-correlation functionals in density functional theory.

Warm dense matter (WDM) – an extreme state of matter characterized by high densities and temperatures – has emerged as one of the most challenging frontiers of plasma physics and material science [1–3]. These conditions occur in many astrophysical objects such as in the interiors of giant planets [4–6], in brown dwarfs [7, 8], and in neutron star crusts [9]. Moreover, they arise in inertial confinement fusion capsules on their pathway towards ignition [10] and are potentially relevant for the understanding of radiation damage in both fission and fusion reactor walls [11]. Furthermore, they apply to the novel field of hot-electron chemistry where the latter are used to accelerate chemical reactions [12, 13].

These applications have sparked a surge of activities in experimental realizations [14] and diagnostics of WDM conditions at intense light sources around the globe, such as at the NIF [15], at SLAC [16], and at the European XFEL [17] which have led to experimental breakthroughs over the last years [18–23]. While all of these experimental techniques rely on theoretical WDM models to extract observables, an accurate theoretical understanding of WDM is yet missing [3, 24].

More specifically, an accurate theoretical description of WDM needs to take into account simultaneously (i) Coulomb coupling effects, (ii) quantum effects, and (iii) thermal excitations. In particular, WDM is characterized by  $r_s \sim \theta \sim 1$ , where  $r_s = \bar{a}/a_B$  and  $\theta = k_B T/E_F$  are the usual Wigner-Seitz radius and degeneracy temperature [25]. Under these conditions, thermal density functional theory (DFT) [26, 27] has emerged as the work-horse of WDM modeling due to its balance between computational cost and accuracy in terms of an –at least formal– *ab initio* treatment of the electrons.

Despite its current success as a useful technique for the numerical modeling of WDM properties, there are potentially severe limitations for further progress: (1) the accuracy of DFT results crucially depends on an accurate exchange-correlation (XC) functional and (2) the computational cost of DFT calculations is too high for on-the-fly diagnostics and interpretation of WDM experiments.

In this regard, the key quantity for WDM diagnostics is the dynamic density response function [28, 29]

$$\chi[G(q, \omega)](q, \omega) = \frac{\chi_0(q, \omega)}{1 - \frac{4\pi}{q^2} (1 - G(q, \omega)) \chi_0(q, \omega)}, \quad (1)$$

where  $\chi_0(q, \omega)$  denotes the density response of a non-interacting (ideal) system and the dynamic local field correction (LFC)  $G(q, \omega)$  entails both the frequency and wave number dependence of XC effects. For example, setting  $G(q, \omega) = 0$  in Eq. (1) leads to the well-known random phase approximation (RPA). An accurate knowledge of Eq. (1) beyond the RPA is paramount for the interpretation of X-ray Thomson scattering (XRTS) experiments [30, 31] that presently constitutes the arguably best diagnostics of WDM experiments.

In addition, the LFC is directly proportional to the XC kernel in time-dependent DFT [32], and, moreover, can be used for the construction of an advanced, non-local XC functional for thermal DFT based on the adiabatic-connection formula and the fluctuation-dissipation theorem [33–35].

Recently, Dornheim and co-workers have presented the first accurate representation of  $G(q, \omega)$  based on *ab initio* path-integral Monte-Carlo (PIMC) data for the warm dense electron gas [36–38]. While a full representation of  $G(q, \omega)$  covering the entire WDM regime currently

remains beyond reach, they have shown that it is often sufficient to replace the dynamic LFC in Eq. (1) by its static limit, i.e.,  $G(q) = G(q, 0)$ . It has, indeed, been demonstrated that this *static approximation*  $\chi^{\text{static}}(q, \omega) = \chi[G(q, 0)](q, \omega)$  yields highly accurate results for the dynamic structure factor (DSF)  $S(q, \omega)$  and related quantities [39]. This is a key finding, as  $G(q)$  is available as a neural-net representation [40] that covers the entire relevant range of  $r_s$  and  $\theta$ .

Yet, as we demonstrate in this Letter, the *static approximation* induces a significant bias for medium to large wave numbers  $q$ , which in turn makes  $\chi^{\text{static}}(q, \omega)$  unsuitable for many applications like the construction of advanced XC functionals for DFT. To overcome this severe limitation, we present the *effective static approximation* (ESA) to the LFC given in Eq. (6). It is constructed on the basis of the machine-learning representation of  $G(q)$  for small  $q$  and, in addition, obeys the consistent asymptotic behaviour in the limit of large wave numbers [41]. Thus, the ESA yields remarkably accurate results for electronic properties like  $S(q, \omega)$ , its normalization  $S(q)$  [Eq. (3)], and the interaction energy  $v$  [Eq. (4)] over the entire WDM regime without any additional computational cost compared to the RPA.

The ESA is, furthermore, directly applicable as a practical method for the rapid diagnostics of XRTS signals. In Fig. 4, we demonstrate its utility for the recent XRTS experiment on isochorically heated aluminum by Sperling *et al.* [42]. We find a significant improvement over standard dielectric models and a remarkable agreement with the experimental data, even when compared to computationally more complex first-principles techniques such as time-dependent DFT.

Finally, the proposed ESA enables wide applications beyond XRTS and XC functionals [24, 43–50].

**Results.** We begin with benchmarking the *static approximation* against accurate QMC results both for the static structure factor (SSF)  $S(q)$  and the interaction energy  $v$ . To this end, we make use of the fluctuation-dissipation theorem [29]

$$S(\mathbf{q}, \omega) = -\frac{\text{Im}\chi(\mathbf{q}, \omega)}{\pi n(1 - e^{-\beta\omega})} \quad (2)$$

which relates the dynamic density response function  $\chi(q, \omega)$  to the DSF  $S(q, \omega)$ , where  $n$  denotes the density and  $\beta$  the inverse temperature. We note that an extensive analysis of the DSF computed within the *static approximation* has been presented elsewhere [36, 37] and need not be repeated here. The corresponding SSF, defined as

$$S(q) = \int_{-\infty}^{\infty} d\omega S(q, \omega), \quad (3)$$

is shown in the top panel of Fig. 1 for the conditions  $r_s = 6$  and  $\theta = 0.5$  which are realized experimentally

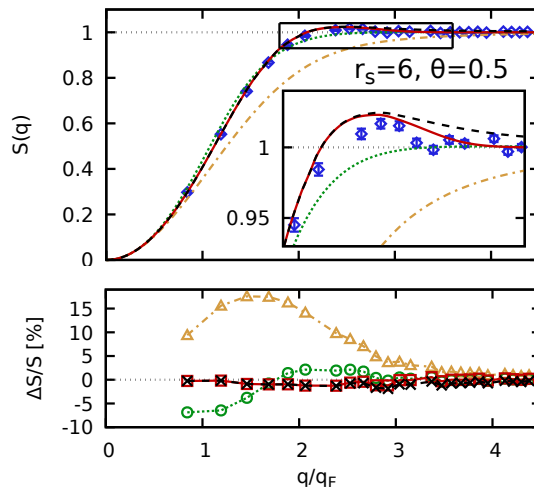


FIG. 1. Top: SSF of the UEG at  $r_s = 6$  and  $\theta = 0.5$ . Blue diamonds: PIMC; solid red: ESA; dashed black: *static approximation*; dotted green: STLS [41, 51]; dash-dotted yellow: RPA. Bottom: Relative deviation from the PIMC results.

in hydrogen jets [52] and evaporation experiments [53–56]. Due to the pronounced impact of electronic XC effects [55], these conditions are challenging from a theoretical perspective and are, therefore, well-suited to benchmark different models. The blue diamonds correspond to PIMC data and are exact within the given error bars. The dashed black line is obtained from the *static approximation* where the exact static limit of  $G(q, \omega)$  available as a neural-net representation [40] was used as input. Remarkably, it is in striking agreement with the exact PIMC results with a maximum deviation of  $\sim 1\%$  (see the bottom panel). As a reference, we also include the SSF computed within the RPA (dash-dotted yellow) and the LFC of Singwi *et al.* [41, 51, 57] (STLS, dotted green). As one might expect, the RPA gives a poor description at these conditions, reflected by the relative deviation exceeding 15%. The STLS formalism is based on an approximate closure relation for  $G(q, 0)$  and leads to a substantial improvement over RPA. Nevertheless, there are still systematic errors: the relative deviation is about 8% and the correlation-induced maximum in  $S(q)$  that appears at  $q \approx 2.2q_F$  is not reproduced by STLS. We thus conclude that the *static approximation* provides a highly accurate description with negligible computational cost even at such challenging conditions; more examples can be found in the Supplemental Material [58].

Let us for now postpone the discussion of the ESA (solid red) in Fig. 1, and investigate the interaction energy of the UEG, computed from  $S(q)$  via [2]

$$v = \frac{1}{\pi} \int_0^{\infty} dq [S(q) - 1]. \quad (4)$$

In Fig. 2 we illustrate the relative accuracy of  $v$  within different theories over the relevant  $\theta$  range and at two

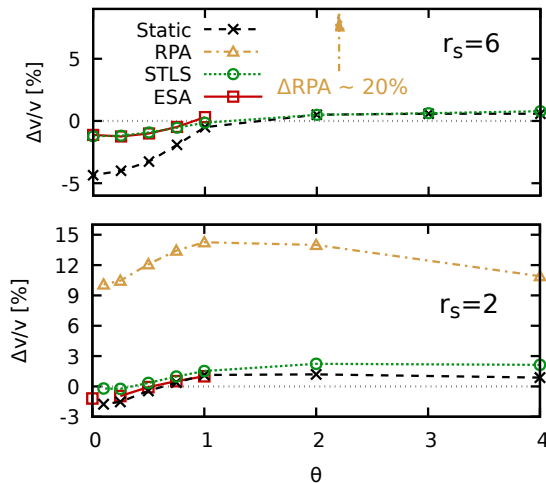


FIG. 2. Relative difference in the interaction energy per particle  $v$  as compared to the accurate parametrization of the exchange–correlation free energy  $f_{xc}$  by Groth *et al.* [59].

relevant values of the density parameter  $r_s$ . The reference result is the QMC-based parametrization by Groth *et al.* [59], which is exact to within  $\sim 0.3\%$ . The top panel corresponds to  $r_s = 6$ , which is most challenging for most theories due to the strong coupling strength. Unsurprisingly, RPA is highly inaccurate over the entire  $\theta$  range with a relative deviation of  $\sim 20\%$ , whereas STLS and the *static approximation* exhibit some interesting behavior: For  $\theta \gtrsim 1$ , both STLS and the *static approximation* are basically exact and can hardly be distinguished from each other. For  $\theta < 1$ , the STLS curve does still not exceed deviations of 2%, whereas the quality of the *static approximation* deteriorates as  $\theta$  decreases with a systematic deviation of almost 5% in the ground state. Let us first consider the comparably high accuracy of STLS for  $v$ . Evidently, this is not due to an inherently correct physical description of the system, as STLS does not reproduce important trends (see Fig. 1). The high accuracy for  $v$  is rather the result of a fortunate cancellation of errors in  $S(q)$  when inserted into Eq. (4), as it is too large in the small- and too low in the high-wave number regime. In contrast, the *static approximation* provides a high-quality description of  $S(q)$  for all  $q$ , but converges too slowly towards unity for large  $q$  (see the inset in Fig. 1). While this bias is relatively small for each individual  $q$  value, the corresponding error in  $v$  accumulates under the integral in Eq. (4) and leads to a substantial bias in the interaction energy.

To develop an improved theory based on the *static approximation* without this obstacle, we have to first understand its origin. Our analysis centers on the well-known asymptotic behaviour of static LFCs [41] for large  $q$

$$\lim_{q \rightarrow \infty} G(q) = 1 - g(0), \quad (5)$$

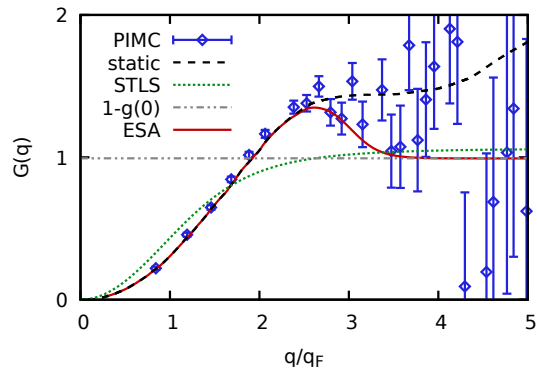


FIG. 3. Wave-number dependence of the local field correction  $G(q)$  at  $r_s = 6$  and  $\theta = 0.5$ . The *static* curve has been obtained from the neural-net given in Ref [40], and the ESA curve corresponds to Eq. (6). The parametrization of the on-top PDF  $g(0)$  is given in the Supplemental Material [58].

where  $g(0)$  is the *on-top* pair distribution function (PDF), i.e., the PDF at zero distance. This is illustrated in Fig. 3, where we show  $G(q, 0)$  again at  $r_s = 6$  and  $\theta = 0.5$ . The dotted green curve corresponds to STLS, which is an example for such a static theory obeying Eq. (5), i.e., it converges towards a constant for large  $q$ . As a side note, we mention that  $G_{\text{STLS}}(q \rightarrow \infty) > 1$ , which leads to an unphysical *negative* value for  $g(0)$ , see also Refs. [29, 60]. The blue diamonds in Fig. 3 have been obtained from a PIMC simulation (see Refs. [40, 61, 62] for details) and are exact within the given error bars. The increasing level of noise towards large  $q$  is due to the reduced impact of  $G(q, \omega)$  [see Eq. (1)], which is further exacerbated by the fermion sign problem [63–65]. Similarly as in Fig. 1, we find that STLS does not give a qualitatively correct description of the  $q$ -dependence, and, in addition, also violates the compressibility sum rule for small  $q$ , see Ref. [51]. The dashed black line depicts the neural-net representation of the exact, *static* LFC from Ref. [40]. While it is in excellent agreement with the PIMC data, it increases monotonically with  $q$  and, thereby, violates the exact limit in Eq. (5).

In fact, it can be shown that this long-wave number behavior of the exact  $G(q, 0)$  is responsible for the unphysically slow convergence of  $S(q)$  towards unity within the *static approximation* [58]. Methods like STLS [41, 51, 57] and other static dielectric theories [66, 67] are based on an LFC independent of  $\omega$ , but still coupled to  $S(q)$  via some form of closure relation. Therefore, these theories do not necessarily constitute an approximation to  $\lim_{\omega \rightarrow 0} G(q, \omega)$ , but can be viewed as a frequency-averaged LFC, i.e., an LFC that is meaningful for quantities that involve a frequency-integral like  $S(q)$  or  $v$ . In contrast, the *static approximation* is based on the exact  $\omega \rightarrow 0$  limit of  $G(q, \omega)$ , which gives remarkably high-quality results for  $S(q, \omega)$  and  $S(q)$ , but induces small, yet significant, unphysical effects that accumulate under

a wave-number integral. In addition to the bias in  $v$ , the slow convergence of  $S(q)$  also induces a divergent on-top PDF [58], and, thus, substantially limits the usefulness of this otherwise powerful parametrization.

To overcome these limitations, we introduce the *effective static approximation* (ESA) as the central result of this paper. It combines the exact  $G(q, 0)$  for  $q \lesssim 3q_F$  with the appropriate long-wave number limit in Eq. (5), thereby, ensuring a proper convergence of  $S(q)$  and the correct on-top PDF  $g(0)$ . The resulting LFC has the form

$$G_{\text{ESA}}(q) = A(q)(1 - g(0)) + G_{\text{nn}}(q)(1 - A(q)), \quad (6)$$

where  $A(q)$  is a simple activation function [58] and  $G_{\text{nn}}(q)$  corresponds to the neural-net from Ref. [40]. We note that the specific form of the activation function is not particularly important for the ESA as long as the conditions  $A(0) = 0$  and  $A(q \rightarrow \infty) = 1$  are satisfied; the empirical choice for  $A(q)$  used in this work is discussed in the Supplemental Material [58]. In addition, we have constructed an analytical parametrization of  $g(0)$  that combines the ground-state results by Spink *et al.* [68] with the restricted PIMC results by Brown *et al.* [69] at finite  $\theta$ . Both the functional form and the corresponding fit parameters are given in the Supplemental Material [58] and can be used for other applications [70–72].

The resulting LFC is shown as the red curve in Fig. 3 and does indeed smoothly combine the exact  $G(q, 0)$  with the consistent limit in Eq. (5). The impact of this improvement is illustrated in Fig. 1, where the ESA reproduces the accurate  $S(q)$  from the *static approximation* for  $q \lesssim 3q_F$ , but, in addition, exhibits a much faster convergence to unity for large  $q$ . As expected, this leads to substantially improved results for integrated quantities, such as interaction energies with an accuracy of  $\sim 1\%$  (Fig. 2). The improved results for  $v$  are also shown at a higher density,  $r_s = 2$ , in the bottom panel of the same figure. Additional results of  $S(q)$  and  $G(q)$  are shown in the Supplemental Material [58].

Up to this point, we have shown that the proposed ESA is capable of yielding highly accurate results for  $S(q, \omega)$ ,  $S(q)$ , and  $v$  without any additional computational cost compared to the RPA.

We conclude this Letter by turning to an actual application of the ESA. We demonstrate its utility as a first-principles method for the rapid interpretation of XRTS signals. Specifically, we consider the XRTS experiment on isochorically heated aluminum by Sperling *et al.* [42] shown in Fig. 4 and demonstrate the impact of electronic XC effects included in the ESA. We compare the deconvolved scattering signal collected from the corresponding XRTS experiment at a scattering angle of  $\theta = 24^\circ$  (black) with several theoretical predictions of the DSF (see Supplemental Material [58] for details). All results are computed within the temperature range from 0.3 to 6.0 eV (where the results for 0.3 eV are depicted as

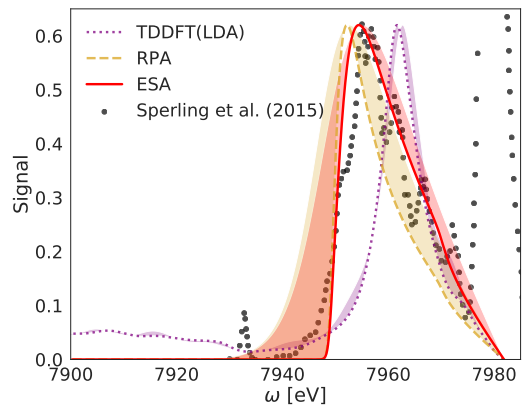


FIG. 4. The deconvolved XRTS signal in isochorically heated aluminum[42] is compared with the DSF from the RPA (yellow), TDDFT (purple), and the ESA (red) are shown in the temperature range from 0.3 to 6.0 eV (0.3 eV in solid). The ESA yields a remarkable agreement with the experimental data, while coming at a computational cost orders of magnitudes lower than TDDFT (about the same as the RPA) [58]. A more extensive discussion of modeling results is given in the Supplementary Material [58].

solid curves). The theoretical predictions are renormalized with respect to the peak at around 7958 eV in the experimental data. The RPA (yellow) and the computationally more complex TDDFT (purple) within the adiabatic LDA yield only qualitative agreement. The ESA (red), however, yields a remarkable agreement with the experimental data, while coming at a computational cost orders of magnitudes lower than TDDFT. Furthermore, in contrast to common, low-cost dielectric models based on phenomenological parameters[27, 57, 73–76], the ESA provides a consistent prediction of XRTS signals from first principles [58].

**Discussion.** In summary, we have presented the ESA which is capable of providing highly accurate results for electronic properties like  $S(q, \omega)$ ,  $S(q)$ , and  $v$ , without any additional computational cost compared to standard RPA calculations. We expect the ESA to replace all known RPA+LFC combinations. The ESA is likely to have tremendous impact in a large number of applications beyond the interpretation of XRTS experiments, such as in the calculation of stopping powers [43, 44], energy relaxation rates [45], and electrical or thermal conductivities [77]. Other examples include the construction of effective potentials [46–48], or the inclusion of electronic correlation effects into other theories like quantum hydrodynamics [24, 49, 50]. Finally, we point out that the ESA is particularly relevant for wave-number averaged quantities like  $v$ , which is of key importance for constructing advanced XC functionals based on the adiabatic-connection formula and the fluctuation-dissipation theorem [33–35]. A python-based implementation of the ESA is freely available online [58] and can be easily incorpo-

rated into existing codes. Moreover, the ESA will be included in a novel open-source XRTS code that is being developed jointly by HZDR and CASUS.

## ACKNOWLEDGMENTS

We acknowledge helpful feedback by M. Bonitz and M. Bussmann.

This work was partly funded by the Center of Advanced Systems Understanding (CASUS) which is financed by the German Federal Ministry of Education and Research (BMBF) and by the Saxon Ministry for Science, Art, and Tourism (SMWK) with tax funds on the basis of the budget approved by the Saxon State Parliament. We gratefully acknowledge computation time on the Bull Cluster at the Center for Information Services and High Performance Computing (ZIH) at Technische Universität Dresden.

---

\* [t.dornheim@hzdr.de](mailto:t.dornheim@hzdr.de)

- [1] V. E. Fortov, “Extreme states of matter on earth and in space,” *Phys.-Usp* **52**, 615–647 (2009).
- [2] T. Dornheim, S. Groth, and M. Bonitz, “The uniform electron gas at warm dense matter conditions,” *Phys. Reports* **744**, 1–86 (2018).
- [3] F. Graziani, M. P. Desjarlais, R. Redmer, and S. B. Trickey, eds., *Frontiers and Challenges in Warm Dense Matter* (Springer, International Publishing, 2014).
- [4] B. Militzer, W. B. Hubbard, J. Vorberger, I. Tamblyn, and S. A. Bonev, “A massive core in jupiter predicted from first-principles simulations,” *The Astrophysical Journal* **688**, L45–L48 (2008).
- [5] J. Vorberger, I. Tamblyn, B. Militzer, and S. A. Bonev, “Hydrogen-helium mixtures in the interiors of giant planets,” *Phys. Rev. B* **75**, 024206 (2007).
- [6] M. Schöttler and R. Redmer, “Ab initio calculation of the miscibility diagram for hydrogen-helium mixtures,” *Phys. Rev. Lett* **120**, 115703 (2018).
- [7] D. Saumon, W. B. Hubbard, G. Chabrier, and H. M. van Horn, “The role of the molecular-metallic transition of hydrogen in the evolution of jupiter, saturn, and brown dwarfs,” *Astrophys. J* **391**, 827–831 (1992).
- [8] A. Becker, W. Lorenzen, J. J. Fortney, N. Nettelmann, M. Schöttler, and R. Redmer, “Ab initio equations of state for hydrogen (h-reos.3) and helium (he-reos.3) and their implications for the interior of brown dwarfs,” *Astrophys. J. Suppl. Ser* **215**, 21 (2014).
- [9] J. Daligault and S. Gupta, “Electron-ion scattering in dense multi-component plasmas: application to the outer crust of an accreting star,” *The Astrophysical Journal* **703**, 994–1011 (2009).
- [10] S. X. Hu, B. Militzer, V. N. Goncharov, and S. Skupsky, “First-principles equation-of-state table of deuterium for inertial confinement fusion applications,” *Phys. Rev. B* **84**, 224109 (2011).
- [11] E. Zarkadoula, S. L. Daraszewicz, D. M. Duffy, M. A. Seaton, I. T. Todorov, K. Nordlund, M. T. Dove, and K. Trachenko, “Electronic effects in high-energy radiation damage in iron,” *J. Phys.: Cond. Matt* **26**, 085401 (2014).
- [12] Shaunak Mukherjee, Florian Libisch, Nicolas Large, Oara Neumann, Lisa V. Brown, Jin Cheng, J. Britt Lassiter, Emily A. Carter, Peter Nordlander, and Naomi J. Halas, “Hot electrons do the impossible: Plasmon-induced dissociation of h2 on au,” *Nano Letters* **13**, 240–247 (2013).
- [13] Mark L. Brongersma, Naomi J. Halas, and Peter Nordlander, “Plasmon-induced hot carrier science and technology,” *Nature Nanotechnology* **10**, 25–34 (2015).
- [14] K. Falk, “Experimental methods for warm dense matter research,” *High Power Laser Sci. Eng* **6**, e59 (2018).
- [15] E. I. Moses, R. N. Boyd, B. A. Remington, C. J. Keane, and R. Al-Ayat, “The national ignition facility: Ushering in a new age for high energy density science,” *Physics of Plasmas* **16**, 041006 (2009).
- [16] Christoph Bostedt, Sébastien Boutet, David M. Fritz, Zhirong Huang, Hae Ja Lee, Henrik T. Lemke, Aymeric Robert, William F. Schlotter, Joshua J. Turner, and Garth J. Williams, “Linac coherent light source: The first five years,” *Rev. Mod. Phys.* **88**, 015007 (2016).
- [17] Thomas Tschentscher, Christian Bressler, Jan Grnert, Anders Madsen, Adrian P. Mancuso, Michael Meyer, Andreas Scherz, Harald Sinn, and Ulf Zastrau, “Photon beam transport and scientific instruments at the european xfel,” *Applied Sciences* **7** (2017), [10.3390/app7060592](https://doi.org/10.3390/app7060592).
- [18] S. H. Glenzer, O. L. Landen, P. Neumayer, R. W. Lee, K. Widmann, S. W. Pollaine, R. J. Wallace, G. Gregori, A. Höll, T. Bornath, R. Thiele, V. Schwarz, W.-D. Kraeft, and R. Redmer, “Observations of plasmons in warm dense matter,” *Phys. Rev. Lett.* **98**, 065002 (2007).
- [19] R. Ernstorfer, M. Harb, C. T. Hebeisen, G. Sciaini, T. Dartigalongue, and R. J. D. Miller, “The formation of warm dense matter: Experimental evidence for electronic bond hardening in gold,” *Science* **323**, 1033 (2009).
- [20] L. B. Fletcher, A. L. Kritcher, A. Pak, T. Ma, T. Döppner, C. Fortmann, L. Divol, O. S. Jones, O. L. Landen, H. A. Scott, J. Vorberger, D. A. Chapman, D. O. Gericke, B. A. Mattern, G. T. Seidler, G. Gregori, R. W. Falcone, and S. H. Glenzer, “Observations of continuum depression in warm dense matter with x-ray thomson scattering,” *Phys. Rev. Lett.* **112**, 145004 (2014).
- [21] M. D. Knudson, M. P. Desjarlais, A. Becker, R. W. Lemke, K. R. Cochrane, M. E. Savage, D. E. Bliss, T. R. Mattsson, and R. Redmer, “Direct observation of an abrupt insulator-to-metal transition in dense liquid deuterium,” *Science* **348**, 1455–1460 (2015).
- [22] D. Kraus, J. Vorberger, A. Pak, N. J. Hartley, L. B. Fletcher, S. Frydrych, E. Galtier, E. J. Gamboa, D. O. Gericke, S. H. Glenzer, E. Granados, M. J. MacDonal, A. J. MacKinnon, E. E. McBride, I. Nam, P. Neumayer, M. Roth, A. M. Saunders, A. K. Schuster, P. Sun, T. van Driel, T. Döppner, and R. W. Falcone, “Formation of diamonds in laser-compressed hydrocarbons at planetary interior conditions,” *Nature Astronomy* **1**, 606–611 (2017).
- [23] S. Frydrych, J. Vorberger, N. J. Hartley, A. K. Schuster, K. Ramakrishna, A. M. Saunders, T. van Driel, R. W. Falcone, L. B. Fletcher, E. Galtier, E. J. Gamboa, S. H. Glenzer, E. Granados, M. J. MacDonal, A. J. MacKinnon, E. E. McBride, I. Nam, P. Neumayer, A. Pak, K. Voigt, M. Roth, P. Sun, D. O. Gericke, T. Döppner,

- and D. Kraus, “Demonstration of x-ray thomson scattering as diagnostics for miscibility in warm dense matter,” *Nature Communications* **11**, 2620 (2020).
- [24] M. Bonitz, T. Dornheim, Zh. A. Moldabekov, S. Zhang, P. Hamann, H. Kählert, A. Filinov, K. Ramakrishna, and J. Vorberger, “Ab initio simulation of warm dense matter,” *Physics of Plasmas* **27**, 042710 (2020).
- [25] Torben Ott, Hauke Thomsen, Jan Willem Abraham, Tobias Dornheim, and Michael Bonitz, “Recent progress in the theory and simulation of strongly correlated plasmas: phase transitions, transport, quantum, and magnetic field effects,” *The European Physical Journal D* **72**, 84 (2018).
- [26] W. Kohn and L. J. Sham, “Self-consistent equations including exchange and correlation effects,” *Phys. Rev.* **140**, A1133–A1138 (1965).
- [27] N. David Mermin, “Thermal properties of the inhomogeneous electron gas,” *Phys. Rev.* **137**, A1441–A1443 (1965).
- [28] A. A. Kugler, “Theory of the local field correction in an electron gas,” *J. Stat. Phys* **12**, 35 (1975).
- [29] G. Giuliani and G. Vignale, *Quantum Theory of the Electron Liquid* (Cambridge University Press, Cambridge, 2008).
- [30] S. H. Glenzer and R. Redmer, “X-ray thomson scattering in high energy density plasmas,” *Rev. Mod. Phys* **81**, 1625 (2009).
- [31] D. Kraus, B. Bachmann, B. Barbrel, R. W. Falcone, L. B. Fletcher, S. Frydrych, E. J. Gamboa, M. Gauthier, D. O. Gericke, S. H. Glenzer, S. Göde, E. Granados, N. J. Hartley, J. Helfrich, H. J. Lee, B. Nagler, A. Ravasio, W. Schumaker, J. Vorberger, and T. Döppner, “Characterizing the ionization potential depression in dense carbon plasmas with high-precision spectrally resolved x-ray scattering,” *Plasma Phys. Control Fusion* **61**, 014015 (2019).
- [32] A. D. Baczewski, L. Shulenburger, M. P. Desjarlais, S. B. Hansen, and R. J. Magyar, “X-ray thomson scattering in warm dense matter without the chihara decomposition,” *Phys. Rev. Lett* **116**, 115004 (2016).
- [33] Christopher E. Patrick and Kristian S. Thygesen, “Adiabatic-connection fluctuation-dissipation dft for the structural properties of solidsthe renormalized alda and electron gas kernels,” *The Journal of Chemical Physics* **143**, 102802 (2015).
- [34] A. Pribram-Jones, P. E. Grabowski, and K. Burke, “Thermal density functional theory: Time-dependent linear response and approximate functionals from the fluctuation-dissipation theorem,” *Phys. Rev. Lett* **116**, 233001 (2016).
- [35] Andreas Görling, “Hierarchies of methods towards the exact kohn-sham correlation energy based on the adiabatic-connection fluctuation-dissipation theorem,” *Phys. Rev. B* **99**, 235120 (2019).
- [36] T. Dornheim, S. Groth, J. Vorberger, and M. Bonitz, “Ab initio path integral Monte Carlo results for the dynamic structure factor of correlated electrons: From the electron liquid to warm dense matter,” *Phys. Rev. Lett.* **121**, 255001 (2018).
- [37] S. Groth, T. Dornheim, and J. Vorberger, “Ab initio path integral Monte Carlo approach to the static and dynamic density response of the uniform electron gas,” *Phys. Rev. B* **99**, 235122 (2019).
- [38] Tobias Dornheim and Jan Vorberger, “Finite-size effects in the reconstruction of dynamic properties from ab initio path integral Monte-Carlo simulations,” arXiv e-prints, arXiv:2004.13429 (2020), [arXiv:2004.13429](https://arxiv.org/abs/2004.13429) [[cond-mat.str-el](https://arxiv.org/abs/2004.13429)].
- [39] Unpublished.
- [40] T. Dornheim, J. Vorberger, S. Groth, N. Hoffmann, Zh.A. Moldabekov, and M. Bonitz, “The static local field correction of the warm dense electron gas: An ab initio path integral Monte Carlo study and machine learning representation,” *J. Chem. Phys* **151**, 194104 (2019).
- [41] S. Tanaka and S. Ichimaru, “Thermodynamics and correlational properties of finite-temperature electron liquids in the Singwi-Tosi-Land-Sjölander approximation,” *J. Phys. Soc. Jpn* **55**, 2278–2289 (1986).
- [42] P. Sperling, E. J. Gamboa, H. J. Lee, H. K. Chung, E. Galtier, Y. Omarbakiyeva, H. Reinholz, G. Röpke, U. Zastrau, J. Hastings, L. B. Fletcher, and S. H. Glenzer, “Free-electron x-ray laser measurements of collisional-damped plasmons in isochorically heated warm dense matter,” *Phys. Rev. Lett.* **115**, 115001 (2015).
- [43] W. Cayzac, A. Frank, A. Ortner, V. Bagnoud, M. M. Basko, S. Bedacht, C. Bläser, A. Blazevic, S. Busold, O. Deppert, J. Ding, M. Ehret, P. Fiala, S. Frydrych, D. O. Gericke, L. Hallo, J. Helfrich, D. Jahn, E. Kjar-tansson, A. Knetsch, D. Kraus, G. Malka, N. W. Neumann, K. Pépitone, D. Pepler, S. Sander, G. Schaumann, T. Schlegel, N. Schroeter, D. Schumacher, M. Seibert, An Tauschwitz, J. Vorberger, F. Wagner, S. Weih, Y. Zobus, and M. Roth, “Experimental discrimination of ion stopping models near the bragg peak in highly ionized matter,” *Nature Communications* **8**, 15693 (2017).
- [44] Zh. A. Moldabekov, T. Dornheim, M. Bonitz, and T. S. Ramazanov, “Ion energy-loss characteristics and friction in a free-electron gas at warm dense matter and non-ideal dense plasma conditions,” *Phys. Rev. E* **101**, 053203 (2020).
- [45] J. Vorberger, D. O. Gericke, Th. Bornath, and M. Schlages, “Energy relaxation in dense, strongly coupled two-temperature plasmas,” *Phys. Rev. E* **81**, 046404 (2010).
- [46] G. Senatore, S. Moroni, and D. M. Ceperley, “Local field factor and effective potentials in liquid metals,” *J. Non-Cryst. Sol* **205-207**, 851–854 (1996).
- [47] Zh.A. Moldabekov, S. Groth, T. Dornheim, H. Kählert, M. Bonitz, and T. S. Ramazanov, “Structural characteristics of strongly coupled ions in a dense quantum plasma,” *Phys. Rev. E* **98**, 023207 (2018).
- [48] Zh.A. Moldabekov, H. Kählert, T. Dornheim, S. Groth, M. Bonitz, and T. S. Ramazanov, “Dynamical structure factor of strongly coupled ions in a dense quantum plasma,” *Phys. Rev. E* **99**, 053203 (2019).
- [49] Abdourahmane Diaw and Michael S. Murillo, “A viscous quantum hydrodynamics model based on dynamic density functional theory,” *Scientific Reports* **7**, 15352 (2017).
- [50] Zh. A. Moldabekov, M. Bonitz, and T. S. Ramazanov, “Theoretical foundations of quantum hydrodynamics for plasmas,” *Physics of Plasmas* **25**, 031903 (2018).
- [51] T. Sjöstrom and J. Dufty, “Uniform electron gas at finite temperatures,” *Phys. Rev. B* **88**, 115123 (2013).
- [52] U. Zastrau, P. Sperling, M. Harmand, A. Becker, T. Bornath, R. Bredow, S. Dzarzhyski, T. Fennel, L. B. Fletcher, E. F”orster, S. G”ode, G. Gregori, V. Hilbert, D. Hochhaus, B. Holst, T. Laarmann, H. J. Lee, T. Ma,

- J. P. Mithen, R. Mitzner, C. D. Murphy, M. Nakatsutsumi, P. Neumayer, A. Przystawik, S. Røling, M. Schulz, B. Siemer, S. Skruszewicz, J. Tiggesbömmker, S. Toleikis, T. Tschentscher, T. White, M. Wöstmann, H. Zacharias, T. Döppner, S. H. Glenzer, and R. Redmer, “Resolving ultrafast heating of dense cryogenic hydrogen,” *Phys. Rev. Lett.* **112**, 105002 (2014).
- [53] J. F. Benage, W. R. Shanahan, and M. S. Murillo, “Electrical resistivity measurements of hot dense aluminum,” *Phys. Rev. Lett.* **83**, 2953 (1999).
- [54] V. V. Karasiev, L. Calderin, and S. B. Trickey, “Importance of finite-temperature exchange correlation for warm dense matter calculations,” *Phys. Rev. E* **93**, 063207 (2016).
- [55] S. Mazevet, M. P. Desjarlais, L. A. Collins, J. D. Kress, and N. H. Magee, “Simulations of the optical properties of warm dense aluminum,” *Phys. Rev. E* **71**, 016409 (2005).
- [56] M. P. Desjarlais, J. D. Kress, and L. A. Collins, “Electrical conductivity for warm, dense aluminum plasmas and liquids,” *Phys. Rev. E* **66**, 025401(R) (2002).
- [57] K. S. Singwi, M. P. Tosi, R. H. Land, and A. Sjölander, “Electron correlations at metallic densities,” *Phys. Rev.* **176**, 589 (1968).
- [58] See Supplemental Material.
- [59] S. Groth, T. Dornheim, T. Sjöström, F. D. Malone, W. M. C. Foulkes, and M. Bonitz, “Ab initio exchange-correlation free energy of the uniform electron gas at warm dense matter conditions,” *Phys. Rev. Lett.* **119**, 135001 (2017).
- [60] Krishan Kumar, Vinayak Garg, and R. K. Moudgil, “Spin-resolved correlations and ground state of a three-dimensional electron gas: Spin-polarization effects,” *Phys. Rev. B* **79**, 115304 (2009).
- [61] Tobias Dornheim, Zhandos A Moldabekov, Jan Vorberger, and Simon Groth, “Ab initio path integral monte carlo simulation of the uniform electron gas in the high energy density regime,” *Plasma Physics and Controlled Fusion* **62**, 075003 (2020).
- [62] Tobias Dornheim, Travis Sjöström, Shigenori Tanaka, and Jan Vorberger, “Strongly coupled electron liquid: Ab initio path integral monte carlo simulations and dielectric theories,” *Phys. Rev. B* **101**, 045129 (2020).
- [63] T. Dornheim, “Fermion sign problem in path integral Monte Carlo simulations: Quantum dots, ultracold atoms, and warm dense matter,” *Phys. Rev. E* **100**, 023307 (2019).
- [64] T. Dornheim, S. Groth, A. V. Filinov, and M. Bonitz, “Path integral monte carlo simulation of degenerate electrons: Permutation-cycle properties,” *The Journal of Chemical Physics* **151**, 014108 (2019).
- [65] M. Troyer and U. J. Wiese, “Computational complexity and fundamental limitations to fermionic quantum Monte Carlo simulations,” *Phys. Rev. Lett.* **94**, 170201 (2005).
- [66] S. Tanaka, “Correlational and thermodynamic properties of finite-temperature electron liquids in the hypernetted-chain approximation,” *J. Chem. Phys.* **145**, 214104 (2016).
- [67] W. Stolzmann and M. Rösler, “Static local-field corrected dielectric and thermodynamic functions,” *Contrib. Plasma Phys.* **41**, 203 (2001).
- [68] G. G. Spink, R. J. Needs, and N. D. Drummond, “Quantum monte carlo study of the three-dimensional spin-polarized homogeneous electron gas,” *Phys. Rev. B* **88**, 085121 (2013).
- [69] Ethan W. Brown, Bryan K. Clark, Jonathan L. DuBois, and David M. Ceperley, “Path-integral monte carlo simulation of the warm dense homogeneous electron gas,” *Phys. Rev. Lett.* **110**, 146405 (2013).
- [70] A. N. Starostin, V. I. Savchenko, and N. J. Fisch, “Effect of quantum uncertainty on the rate of nuclear reactions in the sun,” *Physics Letters A* **274**, 64 – 68 (2000).
- [71] M. Coraddu, M. Lissia, G. Mezzorani, and P. Quarati, “Fusion reactions in plasmas as probe of the high-momentum tail of particle distributions,” *The European Physical Journal B - Condensed Matter and Complex Systems* **50**, 11–15 (2006).
- [72] Travis Sjöström and Jérôme Daligault, “Gradient corrections to the exchange-correlation free energy,” *Phys. Rev. B* **90**, 155109 (2014).
- [73] J. Hubbard and Rudolf Ernst Peierls, “The description of collective motions in terms of many-body perturbation theory,” *Proceedings of the Royal Society of London. Series A. Mathematical and Physical Sciences* **240**, 539–560 (1957).
- [74] Carsten Fortmann, August Wierling, and Gerd Röpke, “Influence of local-field corrections on thomson scattering in collision-dominated two-component plasmas,” *Phys. Rev. E* **81**, 026405 (2010).
- [75] B. B. L. Witte, L. B. Fletcher, E. Galtier, E. Gamboa, H. J. Lee, U. Zastra, R. Redmer, S. H. Glenzer, and P. Sperling, “Warm dense matter demonstrating non-drude conductivity from observations of nonlinear plasmon damping,” *Phys. Rev. Lett.* **118**, 225001 (2017).
- [76] B. B. L. Witte, P. Sperling, M. French, V. Recoules, S. H. Glenzer, and R. Redmer, “Observations of non-linear plasmon damping in dense plasmas,” *Physics of Plasmas* **25**, 056901 (2018).
- [77] H. Reinholz, R. Redmer, G. Röpke, and A. Wierling, “Long-wavelength limit of the dynamical local-field factor and dynamical conductivity of a two-component plasma,” *Phys. Rev. E* **62**, 5648–5666 (2000).